Thermochimica Acta, 163 (1990) 295–302
Elsevier Science Publishers B.V., Amsterdam - Printed in The Netherlands

KINETICS OF NONISOTHERMAL DEHYDRATION OF CRUSHED CRYSTALS OF POTASSIUM COPPER(II) CHLORIDE DIHYDRATE

Haruhiko TANAKA and Nobuyoshi KOGA

Chemistry Laboratory, Faculty of School Education, Hiroshima University, Shinonome, Minami-Ku, Hiroshima, 734 (Japan)

SUMMARY

The internal surfaces of crushed crystals of $K_2CuCl_4 \cdot 2H_2O$, dehydrated nonisothermally to various reaction fractions, were observed using a polarizing microscope. The reaction proceeds inward, through the advancement of reaction fronts, and is accompanied by some random nucleation in the bulk. The results are compared with those for the nonisothermal dehydration of single crystal $K_2CuCl_4 \cdot 2H_2O$ [J. Phys. Chem., 92(1988)7023]. A marked difference in kinetic behavior between the two samples is explained by assuming that diffusion of the gaseous product is impeded by the outerlayer of the crystalline product. Mathematical analyses of the simultaneous TG and DSC traces at various heating rates suggest that the reaction, as a whole, is regulated by a contracting geometry law. However, an Avrami-Erofeyev law plays an important role in the early stage of the dehydration. Comparison of kinetic results, assessed from TG and DSC, favors the above assumption that the gaseous diffusion is a rate determining step, particularly at the later stages of reaction.

INTRODUCTION

Many chemical reactions occurring within solids proceed preferentially at a reaction interface, characterized as a zone of locally enhanced reactivity of reactant-product contacts. In addition to kinetic analyses of the thermoanalytical (TA) curves, direct observation of samples partially decomposed is valuable in determining kinetic mechanisms of solid-state decompositions (refs. 1-4).

The present paper reports the kinetics of the nonisothermal dehydration of crushed crystals of potassium copper(II) chloride dihydrate (PCCD) to establish the characteristic rate behavior by use of two experimental approaches. One is direct observation of internal surfaces of partially dehydrated PCCD powders by using the thin section technique (refs. 4, 5). The other is kinetic analyses of the TG and DSC traces recorded simultaneously and a comparison of kinetic results obtained from these two TA curves. It was hoped that the two approaches can provide us with a wider comprehension of complex mechanistic features of solid-state reactions at the fundamental level.

0040-6031/90/$03.50 © 1990 Elsevier Science Publishers B.V.

EXPERIMENTAL

Simultaneous TG-DSC traces for the nonisothermal dehydration of crushed crystals of PCCD of various particle-size fractions, which were prepared as described previously (ref. 6), were analyzed to compare kinetic results derived from TG and DSC. The DSC traces were integrated to produce curves of the fractional reaction, α, versus the temperature, T, by using a microcomputer and analyzed kinetically.

The crushed crystals of a -24+48 mesh sieve fraction were prepared from single crystals. These were dehydrated nonisothermally to different α values under conditions identical to the TA measurements. Thin sections of the partially dehydrated samples were prepared in a similar way to those of the single crystals (refs. 4-6). The internal surfaces were observed using a polarizing microscope and photographed.

RESULTS AND DISCUSSION

Figure 1 shows representative polarizing microscopic views of the internal surfaces of a 60%-dehydrated sample of the -24+48 mesh sieve fraction, which was dehydrated at a heating rate β of 1.00 K/min. We see from Fig. 1, as expected, that the fractional reaction α is an average over all the particles examined, in which α is different depending on the particle. It is likely that the reaction initially proceeds through superficial nucleation and its growth which then advances inward. The reaction interfaces are not plain, which is far from the theoretical model. We also see that advancement of the growth front is accompanied by some random nucleation and growth in the bulk.

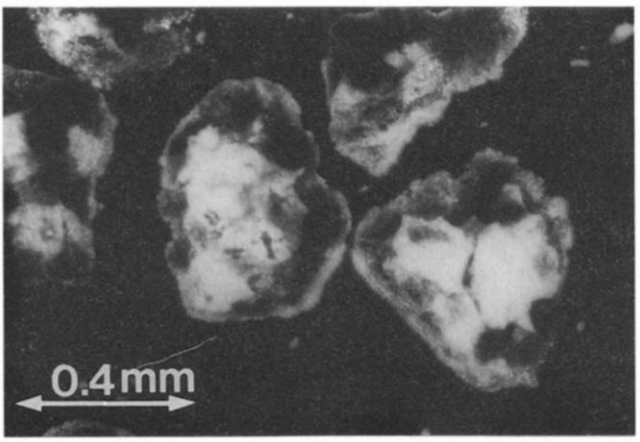

Fig. 1. Typical polarizing microscopic view of the internal surfaces of 60%-dehydrated crushed crystals of PCCD of a -24+48 mesh sieve fraction.

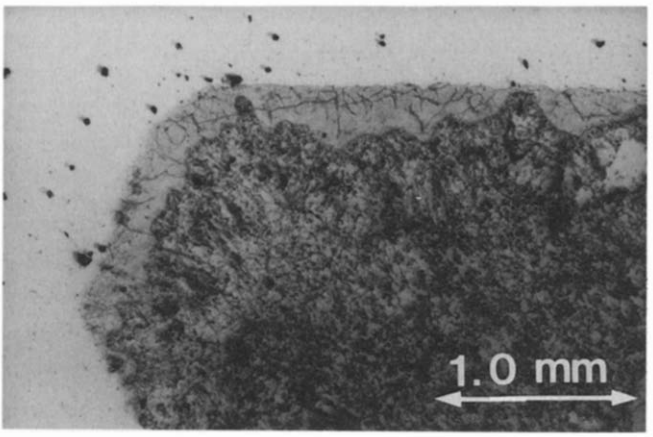

Fig. 2. Typical polarizing microscopic view of an internal (100) surface of a 70%-dehydrated single crystal of PCCD.

It is interesting to link the present observation with that of the single crystal material (ref. 6). Figure 2 shows, for comparison, a representative polarizing microscopic view of an internal (100) surface of a 70%-dehydrated single crystalline PCCD. A marked difference between the two samples is that the outerlayer of the crystalline product impedes the escape of evolved water vapor from the interior of the single crystal sample, whereas this is much easier for the crushed crystals. This is one of the reasons why the dehydration of the powdered PCCD is much faster than that of the single crystal material. Another reason for the faster reaction is that this reaction proceeds, more or less, according to a contracting geometry law, R_n, in which the rate constant k increases with decreasing particle size.

It is worth relating the above result with the rate data obtained from the analysis of simultaneous TG-DSC measurements. Figure 3 shows the typical TG and integrated DSC curves for nonisothermal dehydration of powdered PCCD of the particle-size fractions of -100+170, -48+100, and -24+48 mesh at various β values. During the initial and main part of the reaction ($\alpha < 0.8$), almost no distinct lag between these two traces results with the smallest particle-size fraction, -100+170 mesh. With larger particle-size fractions of -48+100 and -24+48 mesh, however, TG curves shift to higher temperature regions, which becomes increasingly marked as reaction advances. This is possibly because diffusion of water vapor through the solid-product layer (see Fig. 1) is more difficult for larger particle-size fractions. In addition, the temperature differences between these two curves at a given α value increased with increasing β. This trend could be explained if the increase in the rate of advancement of the reaction interface, caused by the increase in β, is much

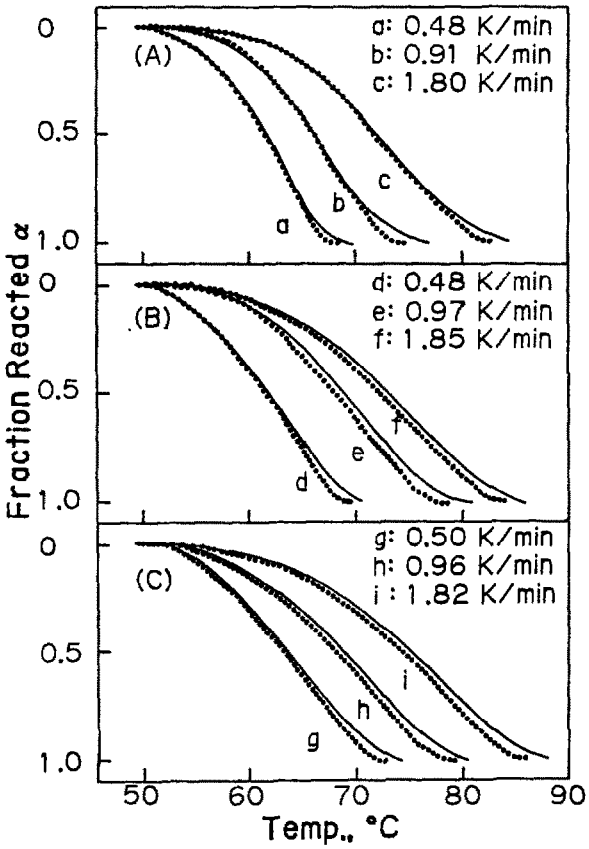

Fig. 3. Typical TG(———) and integrated DSC(••••••) curves of nonisothermal dehydration of crushed crystals of PCCD of particle-size fractions: (A) -100+170; (B) -48+100; and (C) -24+48 mesh.

more marked than the corresponding increase in the rate of diffusion of the water vapor through the solid product (ref. 7). Another factor could be that more rapid crystallization of the product at higher reaction temperatures impedes the escape of water vapor through the product phase (ref. 8).

During the later stage of the reaction ($\alpha > 0.8$), all the TG curves shift to higher temperatures at a given α value than the integrated DSC curves. The tail of the TG curves seems to be caused by slower escape of water vapor and by the reverse reaction. On the other hand, the DSC curves are recorded in response to a total enthalpy change including, for instance, endotherms due to breaking of chemical bonds, diffusion and desorption of water vapor and an exotherm due to crystallization of the solid product. Table 1 lists the peak temperature of the DSC curves, together with that of the DTG curves obtained by differentiating the TG traces. The peak temperatures of DSC are higher than

TABLE 1

Effects of heating rate and particle size on the peak temperatures for the nonisothermal dehydration of PCCD.

Particle-size fraction, mesh	Curve	Peak temperature, ℃ Heating rate, K/min 0.49±0.01	0.95±0.01	1.83±0.01
-100+170	DSC	63.8±0.3	69.8±0.3	77.2±0.1
	DTG	62.1±0.2	68.5±0.2	74.1±0.2
-48+100	DSC	65.6±0.3	72.7±0.2	77.7±0.2
	DTG	63.5±0.3	71.5±0.3	75.3±0.2
-24+48	DSC	67.5±0.3	72.9±0.1	79.4±0.1
	DTG	64.8±0.2	72.0±0.2	76.3±0.1

those of DTG. This is because the peaks of the DSC and DTG curves were observed at $0.70 < \alpha < 0.75$ and $0.55 < \alpha < 0.60$, respectively.

Mathematical analysis was made for the TA curves at β lower than 3.40 K/min, because a splitting of the DSC peak was observed at higher β (ref. 6). The splitting of the DSC peak seems to correspond to the "arrest (ref. 9)" of the reaction and be closely connected with the difficulty of the gaseous diffusion which is impeded by more rapid crystallization of a solid-product layer at higher β. The TG and integrated DSC curves were analyzed by the Ozawa method (ref. 10) with $p(x) \fallingdotseq \exp(-x)/x^2$ (ref. 11). Figure 4 shows the activation

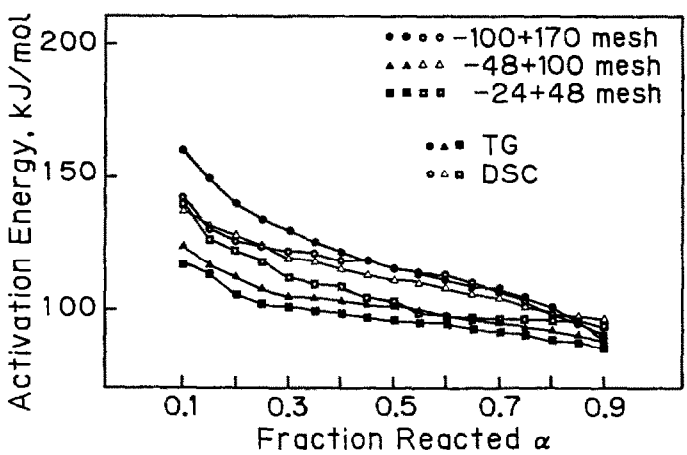

Fig. 4. Activation energies, E, at various fractions reacted, α, derived, in terms of the TG and integrated DSC curves by the Ozawa method, for the non-isothermal dehydration of crushed crystals of PCCD at different heating rates.

energies E, derived in terms of the TG and integrated DSC curves, at various α values from 0.10 to 0.90 in steps of 0.05 for the nonisothermal dehydration of crushed crystals of PCCD of various particle-size fractions. We see from Fig. 4 that for the smallest particle-size fraction, -100+170 mesh, the E values calculated from the integrated DSC curves are smaller than those from the TG traces. On the contrary, the reverse is true for the larger particle-size fractions. We also see from Fig. 4 that the values of E from both the TG and integrated DSC curves decrease with increasing α, particularly at smaller α ($\alpha < 0.3$) for all the particle-size fractions examined.

Estimation of the kinetic rate function $F(\alpha)$ and the preexponential factor A from the Ozawa method is generally supposed to be valid only if the apparent value of E is constant at different α. On the other hand, the variation in E also suggests a possibility of change in the kinetic obedience during the course of reaction. It is interesting here to evaluate these parameters within various restricted ranges of α, in which the variation in E is smaller, in an attempt to detect the change in rate behavior depending on α (ref. 12). Table 2 lists the most appropriate $F(\alpha)$ and Arrhenius parameters obtained from the Ozawa method in various restricted ranges of α. We see that

TABLE 2

Comparison of the kinetic parameters, $F(\alpha)$, E and logA, derived by the Ozawa method for the nonisothermal dehydration of powdered PCCD.

Particle size fraction, mesh	Range of α	TG				Integrated DSC			
		$F(\alpha)$	E, kJ/mol	logA, 1/s	γ*	$F(\alpha)$	E, kJ/mol	logA, 1/s	γ*
-100+170	0.1-0.9	$R_{3.3}$	124	15.7	0.9999	$R_{2.7}$	115	14.5	0.9998
	0.1-0.5	$A_{1.1}$	136	18.2	0.9999	$A_{1.4}$	125	16.5	0.9999
	0.2-0.6	$A_{1.2}$	127	16.8	0.9999	$A_{1.3}$	120	15.7	0.9999
	0.3-0.7	$A_{1.2}$	121	15.9	0.9999	$A_{1.3}$	116	15.1	0.9999
	0.4-0.8	$R_{3.3}$	116	14.5	0.9999	$R_{3.1}$	112	13.9	0.9999
	0.5-0.9	$R_{2.5}$	110	13.8	0.9999	$R_{2.6}$	106	13.1	0.9999
-48+100	0.1-0.9	$R_{2.3}$	103	12.5	0.9999	$R_{2.9}$	114	14.1	0.9999
	0.1-0.5	$A_{1.0}$	110	14.0	0.9996	$A_{1.1}$	123	16.1	0.9999
	0.2-0.6	$A_{1.3}$	105	13.2	0.9998	$A_{1.2}$	117	15.2	0.9999
	0.3-0.7	$R_{1.7}$	101	12.4	0.9998	$A_{1.2}$	112	14.5	0.9999
	0.4-0.8	$R_{2.5}$	99	11.9	0.9999	$R_{2.7}$	109	13.4	0.9999
	0.5-0.9	$R_{2.3}$	96	11.5	0.9999	$R_{2.1}$	105	12.8	0.9999
-24+48	0.1-0.9	$R_{2.4}$	98	11.7	0.9999	$R_{2.4}$	107	13.1	0.9998
	0.1-0.5	$A_{1.1}$	104	13.1	0.9999	$A_{1.0}$	117	15.0	0.9998
	0.2-0.6	$A_{1.2}$	100	12.4	0.9998	$A_{1.0}$	109	13.8	0.9999
	0.3-0.7	$R_{1.9}$	97	11.6	0.9999	$R_{2.7}$	104	12.5	0.9998
	0.4-0.8	$R_{2.2}$	95	11.2	0.9999	$R_{1.8}$	100	12.1	0.9999
	0.5-0.9	$R_{2.6}$	93	10.8	0.9999	$R_{1.8}$	98	11.6	0.9999

* Correlation coefficient of the linear regression analysis of the $F(\alpha)$ vs. θ plot.

TABLE 3

The Arrhenius parameters calculated, within a restricted α range of 0.70-0.99 in terms of the R_3 and D_3 laws, by the CR method for the TG traces for the non-isothermal dehydration of powdered PCCD .

Particle size fraction, mesh	Heating rate, K/min	$R_3=1-(1-\alpha)^{1/3}$ E, kJ/mol	logA, 1/s	$-\gamma$*	$D_3=[1-(1-\alpha)^{1/3}]^2$ E, kJ/mol	logA, 1/s	$-\gamma$*
-100+170	0.50	177	24.2	0.9874	358	52.1	0.9850
	0.94	134	17.3	0.9895	274	38.4	0.9910
	1.84	134	17.2	0.9952	273	37.9	0.9966
-48+100	0.48	130	16.7	0.9907	266	37.5	0.9923
	0.95	135	17.4	0.9939	276	38.6	0.9920
	1.89	99	11.8	0.9887	203	27.2	0.9906
-24+48	0.50	127	16.2	0.9892	259	36.3	0.9895
	0.96	121	15.3	0.9910	248	34.3	0.9912
	1.84	66	6.7	0.9876	138	17.3	0.9934

* Correlation coefficient of the linear regression analysis of the CR plot.

kinetic obedience to the A_n law with $n \fallingdotseq 1$ was observed at an early stage of reaction. This implies that superficial nucleation and growth of these nuclei play an important role at this stage. At the same time, distribution of α among the particles in a pan seems to be responsible for the apparent kinetic obedience to the A_n law. The succeeding stage of reaction is well described by R_n laws, although the value of n varies with the particle size, range of α and TA method. We ascribe the variation in the n value to partial participation of random nucleation and its growth in the bulk, as seen from Fig. 1, and of diffusion of gaseous products.

The later stage of the reaction ($0.70 < \alpha < 0.99$) was also analyzed kinetically by using the Coats & Redfern (CR) method (ref. 13). Table 3 shows a comparison of the Arrhenius parameters and correlation coefficient of linear regression analysis of the CR plot, calculated in terms of the R_3 and D_3 laws, for the TG traces within a restricted α range of 0.70-0.99. We see from Table 3 that in the later stage the D_3 law is more representative than the R_3 law. The tendency is marked at higher β and for the larger particle sizes. This also supports the above suggestion that the reaction rate at the later stage is regulated by the diffusion of water vapor through the solid product.

We also see from Tables 2 and 3 that there is some variation in the Arrhenius parameters depending on the range of α, TA method, particle size and β. These parameters show kinetic compensation behavior (ref. 14). This is in good agreement with the general trend that the kinetic compensation behavior is observed whenever the TA traces shift along the temperature coordinate

accompanied by a change in the slope (refs. 14, 15).

CONCLUSION

The nonisothermal dehydration of powdered PCCD in flowing N_2 initially proceeds through superficial nucleation and its growth. During the early stage of reaction (ca. α <0.3), the rate data obey an Avrami-Erofeyev law, A_m, with $m \fallingdotseq 1$. The tendency increases with decreasing particle size. Time lags in reaction initiation among the particles in a pan are also responsible for the obedience to the A_m law. The succeeding stage ($0.3<\alpha<0.8$) is regulated by a phase boundary controlled law, R_n, with $2<n<3$. This is in agreement with the microscopic observation that the geometry of the interface developed during the dehydration is roughly represented by a contracting volume model. It is suggested that, as the reaction advances (in particular $\alpha > 0.8$), diffusion of water vapor produced at reaction fronts through the product layer becomes difficult. This is much more marked for the larger particle sizes. As a result of such complex behavior, the n value in the R_n law seems to vary depending on the particle size, range of α and TA method.

REFERENCES

1 A.K. Galwey, R. Reed, and G.G.T. Guarini, Observations on internal structures of chrome alum dehydration nuclei, Nature, 283(1980)52-54.
2 G.G.T. Guarini and S. Piccini, The dehydration of $Na_2S_2O_3 \cdot 5H_2O$ single crystals as studied by thermal analysis and optical microscopy, J. Chem. Soc. Faraday Trans. 1, 84(1988)331-342.
3 M.E. Brown, Quantitative Thermoanalytical studies of the kinetics and mechanisms of the thermal decomposition of inorganic solids, Thermochim. Acta, 110(1987)153-158.
4 H. Tanaka and N. Koga, Polarizing microscopy for examining mechanisms of the decomposition of single crystal materials, Thermochim. Acta, 133(1988) 227-232.
5 H. Tanaka, Y. Yabuta, and N. Koga, Kinetic study of the dehydration of sodium citrate dihydrate, React. Solids, 2(1986)169-175.
6 H. Tanaka and N. Koga, Kinetics of the thermal dehydration of potassium copper(II) chloride dihydrate, J. Phys. Chem., 92(1988)7023-7029.
7 N. Koga and H. Tanaka, Kinetic study of the thermal dehydration of copper(II) acetate monohydrate I. Single crystal material, submitted.
8 G.G.T. Guarini and A. Magnani, Photoacoustic evidence of the formation of a dehydrated surface layer during the initial stages of the dehydration of α-$NiSO_4 \cdot 6H_2O$, React. Solids, 6(1988)277-280.
9 N.Z. Lyakhov and V.V. Boldyrev, Kinetics and mechanism of the dehydration of crystal hydrates, Russ. Chem. Reviews, 41(1972)919-928.
10 T. Ozawa, A new method of analyzing thermogravimetric data, Bull. Chem. Soc. Jpn., 38(1965)1881-1886.
11 C.D. Doyle, Series approximations to the equation of thermogravimetric data, Nature, 207(1965)290-291.
12 N. Koga and H. Tanaka, Kinetics and mechanisms of the thermal dehydration of $Li_2SO_4 \cdot H_2O$, J. Phys. Chem., in press.
13 A.W. Coats and J.P. Redfern, Kinetic parameters from thermogravimetric data, Nature, 201(1964)68-69.
14 J. Zsako, The kinetic compensation effect, J.Therm.Anal., 9(1976)101-108.
15 N. Koga and H. Tanaka, Significance of kinetic compensation effect in the thermal decomposition of a solid, Thermochim. Acta, 135(1988)79-84.